An Efficient Correction Storage Scheme for Unsteady Flows

Jo-Soon Cheong, Youn J. Kim*
School of Mechanical Engineering, Sungkunkwan University

An efficient correction storage scheme on a structured grid is applied to a sequence of approximate Jacobian systems arising at each time step from a linearization of the discrete nonlinear system of equations, obtained by the implicit time discretization of the conservation laws for unsteady fluid flows. The contribution of freezing the Jacobian matrix to computing costs is investigated within the correction storage scheme. The performance of the procedure is exhibited by measuring CPU time required to obtain a fully developed laminar vortex shedding flow past a circular cylinder, and is compared with that of a collective iterative method on a single grid. In addition, some computed results of the flow are presented in terms of some functionals along with measured data. The computational test shows that the computing costs may be saved in favor of the correction storage scheme with the frozen Jacobian matrix, to a great extent.

Key Words : Conservation Laws, Implicit Scheme, Correction Storage Scheme, Computing Costs, Frozen Jacobian Matrix, Riemann Solver, Unsteady Flow, Vortex Shedding

1. Introduction

The majority of flows in nature or technical applications, suffering from some form of perturbations, are essentially unsteady, e. g. the evolution with time of boundary layers, separation, reattachment, vortex shedding and interaction in turbomachinery blade rows, etc.. Such flow phenomena may be induced either by external or self excitation or by a combination of both excitations. Vortex shedding from bluff bodies is a typical unsteady phenomenon induced by self excitation, while the sources of the unsteadiness in turbomachinery blade rows are complex.

To date, the numerical solution of the conservation laws for fluid flows has, however, concentrated largely on steady state problems because of the constraints of computing costs. The evolution of high performance computer resources now somewhat enables us to look into the characteristics of time evolution flows. The numerical simulation of unsteady flows requires high accuracy in time as well as in space. Unlike steady flow problems, higher grid resolution is required to capture the details of unsteady flows accurately since the discretization errors coupled in space and time increase with lapse of time.

Following the method of lines, the discretization of the conservation laws in space first leads to a nonlinear system of first order ordinary differential equations, so-called semi-discrete representation. With regard to the implicit time integration of the representation, a nonlinear system of algebraic equations has to be iteratively solved for time accurate solutions at each time cycle.

To overcome such difficulty in solving such a nonlinear system arising at each implicit time step, or to transform an explicit code for steady flows present straightforwardly into a code for unsteady ones, Jameson (1991) and Dailey et al.

* Corresponding Author,
E-mail : kimyj@me.skku.ac.kr
TEL : +82-31-290-7448 ; **FAX** : +82-31-290-5849
School of Mechanical Engineering, Sungkyunkwan University, 300 Chunchun-dong, Jangan-gu, Suwon, Kyunggi-do 440-746, Korea. (Manuscript **Received** June 12, 2000; **Revised** October 19, 2000)

(1996) added an artificial time derivative to a nonlinear system. They then solved the resulting artificial time dependent system within the context of a multigrid methodology (a full approximation storage scheme) with use of a psuedo-explicit Runge-Kutta time stepping scheme (often called the dual time stepping) as a smoother. However, they discretized the convective spatial derivative terms centrally, for implicit schemes resulting in the coefficient-matrix that was not good-conditioned to solve the linear systems of equations with use of iterative methods. This technique is widely in use for computation of unsteady flows, for example, by Breuer et al. (1993). However, this psuedo-time stepping technique also suffers a limitation on the artificial time step size as in the case of real explicit time stepping.

Implicit schemes also have been employed successfully by many investigators for simulation of unsteady flows. Rai (1989) and Jiang et al. (1995) solved the Jacobian systems obtained by linearization of a nonlinear system with use of an iterative procedure, while Sheng et al. (1995), Pulliam (1993) added an artificial time derivative to a nonlinear system and then solved the resulting time dependent system with aid of a non-iterative implicit scheme for steady flows. They all attacked the Jacobian systems in terms of an iterative, approximate factorization or conjugate gradient-type method on a single grid. However, a few investigators have reported the application of the multigrid method to the Jacobian systems for simulation of unsteady flows.

The effectiveness of the implicit scheme depends strongly on the efficiency of the linear solver used for the Jacobian systems. The goal of this article is in developing an efficient correction storage scheme for solving the Jacobian systems within an implicit time integration for simulating unsteady flows. The difficulty in applying structured meshes to complex configurations may be considerably relieved by resorting to unstructured meshes. However, the main question appears to be the inherent efficiency limitations of unstructured flow solvers, compared with structured ones. The efficiency of a multigrid method is strongly affected by the solution procedure employed on a single grid, but playing the role of a smoother in the multigrid context. It thus appears to be evident that the multigrid method on unstructured meshes is not so efficient as that on structured ones. In the current work, the efficiency of a correction storage scheme will be evaluated on a structured grid.

Since the first order approximate Riemann solver for an implicit operator in linearized form provides a good-conditioned coefficient-matrix for collective iterative methods, an iterative method of some type also may be chosen to solve the Jacobian systems. Another possibility is to find the solution errors of the Jacobian systems, obtained by performing a few iterations on the finest grid, on coarser grids, known as the correction storage scheme, where computing costs are much cheaper.

For the case of a modified Newton-Raphson method in which the Jacobian matrix is not updated and factorized at each Newton-Raphson step, the Jacobian matrix evaluated once may be reused during the linear iterative processes of each time cycle. This would reduce the overall computing time since, for the Jacobian matrix evaluated once at the beginning, the splitting matrix of the collective linear iterative method used needs not to be factorized repeatedly. In addition, the technique of freezing the Jacobian matrix may be incorporated into the correction storage scheme. In the current work, the effectiveness of these techniques is tested to evaluate the effect on computing costs.

The test case chosen is the two-dimensional unsteady laminar flow over a circular cylinder that moves with some constant translational velocity following an impulsive start from rest. As computed results, following the presentation of some numerical functionals for the symmetric and asymmetric flows along with measured data, the effectiveness of the correction storage scheme to efficiently resolve unsteady flows are estimated for the asymmetric flow through a comparison with other methods.

2. Mathematical Modeling

The flow of a continuum is described by the conservation laws for mass, momentum and energy. Body forces are not taken into account here. Considering a control volume V of interest fixed in time and space, with the outward unit vector $\underline{n}$ being normal to the control volume surface S surrounding the volume, in an absolute frame of reference, the conservation laws in integral form read:

$$\int_c \frac{\partial \underline{Q}}{\partial t} dV + \int_s (\underline{\underline{F}}^c - \underline{\underline{F}}^v) \cdot \underline{n} dS = 0 \qquad (1)$$

where

$$\underline{Q} = \begin{bmatrix} \rho \\ \rho \underline{u} \\ \rho E \end{bmatrix}, \quad \underline{\underline{F}}^c = \begin{bmatrix} \rho \underline{u} \\ \rho \underline{u}\underline{u} + pI \\ (\rho E + p)\underline{u} \end{bmatrix},$$

$$\underline{\underline{F}}^v = \begin{bmatrix} 0 \\ \underline{\underline{T}} \\ \underline{\underline{T}} \cdot \underline{u} - \underline{q} \end{bmatrix}.$$

In the above relations, the vector $\underline{Q}$ states for the conservative variables at the current time t, i. e. the mass density ρ, the momentum density $\rho \underline{u}$ and the total internal energy density ρE. and $\underline{\underline{F}}^c$ represent $\underline{\underline{F}}^v$ the convective and the diffusive flux contributions to the flux tensor $\underline{\underline{F}}$. I and $\underline{u}$ are the unit tensor and the velocity vector, respectively. The convective flux tensor $\underline{\underline{F}}^c$ depends only on the vector $\underline{Q}$, while the diffusive flux tensor depends mainly on the gradients of $\underline{Q}$.

For a fluid obeying the Newton's law and Stokes's hypothesis for the bulk viscosity, an expression for the molecular viscous stress tensor $\underline{\underline{T}}$ is given by

$$\underline{\underline{T}} = \mu \left[\nabla \underline{u} + (\nabla \underline{u})^T - \frac{2}{3} \nabla \cdot \underline{u} I \right] \qquad (2)$$

and the Fourier's law states for the heat flux vector $\underline{q}$ by conduction through the control surface

$$\underline{q} = -\lambda \nabla T \qquad (3)$$

where ∇ is the gradient operator and the superscript T the transpose. In this work, the flow is assumed to be laminar. The Prandtl number, giving a relationship between the molecular thermal conductivity λ and the dynamic viscosity μ, assumed to be constant, namely $Pr = 0.72$ as well. The dependence of the viscosity μ on the static temperature T is obtained from the Sutherland's law.

For a thermally and calorically ideal gas with the constant specific heat ratio γ and the gas constant R, the static pressure p and the static temperature T are related to the equations of state:

$$p = (\gamma - 1)\left[\rho E - \frac{\rho}{2} \underline{u} \cdot \underline{u} \right], \quad T = \frac{p}{\rho R} \qquad (4)$$

The conservation laws of Eq. (1) are put into a nondimensional form with reference values, denoted with ∞. Length is nondimensionalized by L_∞, $\underline{u}$ by U_∞, ρ by ρ_∞, T by T_∞, t by L_∞, ρ by $\rho_\infty U_\infty^2$ and μ by μ_∞. From here on, all the physical variables are thus dimensionless except for reference values, unless otherwise stated.

3. Numerical Formulation

Let the control volume V be divided into a number of cells forming grids. Since Eq. (1) is valid for any arbitrary control volume, it also holds locally for each individual cell in a grid. By the mean-value theorem, the conservation laws for a cell with a volume of ΔV, being not a function of time t, become:

$$\Delta V \frac{d\tilde{Q}}{dt} + \sum_i \underline{\underline{F}}(\tilde{Q}) \cdot \underline{S}^i = 0 \qquad (5)$$

where $\tilde{Q}$ is the cell-averaged value located at the center of the cell, and $\underline{\underline{F}}(\tilde{Q}) \cdot \underline{S}^i$ is the corresponding flux at each surface $\underline{S}^i$ of ΔV. The superscript i denotes the contravariant component.

Since $\tilde{Q}$ is located in the center of the cell, but $\underline{\underline{F}}(\tilde{Q})$ at its surfaces, some interpolation (or extrapolation) of the neighboring dependent variables must be performed to obtain the discrete solution of Eq. (5). The flux tensor thus determined will be called the numerical flux tensor $\underline{\underline{\tilde{F}}}(\tilde{Q})$. Introducing a unit vector $\underline{e}^i$ with the same direction as $\underline{S}^i$ and using the norm S^i of $\underline{S}^i$, then Eq. (5) becomes

$$\Delta V\frac{d\tilde{Q}}{dt}+\sum_i \tilde{f}^i(\tilde{Q})S^i=0, \tag{6}$$

where $\tilde{f}^i(\tilde{Q})=\tilde{\underline{F}}(\tilde{Q})\cdot g^i$ is called the numerical flux vector.

Eq. (6) is a form of the finite volume method for the conservation laws. The accuracy of the vector $\tilde{Q}$ depends largely on the quality of the evaluation scheme for the numerical flux vector $\tilde{f}^i(\tilde{Q})$. An evaluation scheme used here for the numerical flux function will be briefly described in the following.

3.1 Evaluation of numerical fluxes

The scheme used for evaluating the numerical flux vector $\tilde{f}^i(\tilde{Q})$ is based on the state difference splitting of the form

$$\tilde{f}^i(\tilde{Q})=\tilde{\underline{F}}^C(\tilde{Q}^*)\cdot g^i-\tilde{\underline{F}}^D\cdot g^i \tag{7}$$

where $\tilde{Q}^*$ is the intermediate state vector at the cell surface (Osher et al., 1982).

The intermediate state vector $\tilde{Q}^*$ is calculated from the two states that are interpolated from the two different sets of neighboring grid points, i. e. $\tilde{Q}^+=\tilde{Q}^+(\tilde{Q}_L, \tilde{Q}_R, \tilde{Q}_{R+1})$ and $\tilde{Q}^-=\tilde{Q}^-(\tilde{Q}_{L-1}, \tilde{Q}_L, \tilde{Q}_R)$. The subscripts L and R denote the values from the left (L) and right (R) cells sharing S^i. The interpolation is carried out using the limiter function after van Albada (1982). It is done in characteristic variables $\tilde{Q}_{\tilde{\alpha}}$, which are those components of the vector $\tilde{Q}$, to which known propagation speeds $\lambda_c(\tilde{\alpha})$ can be related. They are generated by a proper choice of base vectors $g^{\tilde{\alpha}}$ and $g_{\tilde{\alpha}}$. These base vectors and the propagation speeds are evaluated using the density weighted average proposed by Roe (1981). The subscript $\tilde{\alpha}$ and the superscript $\tilde{\alpha}$ denote the covariant and the contravariant characteristic components, respectively.

The differences between the two states $\tilde{Q}^+$ and $\tilde{Q}^-$ are regarded as waves propagating in different directions corresponding to their propagation speeds. The state vector $\tilde{Q}^*$, needed to calculate the flux vector at a cell surface, is composed of those wave components, which propagate towards the cell surface. The intermediate state may be found by following a path connecting the two states $\tilde{Q}^+$ and $\tilde{Q}^-$, and by looking for the change of sign of the actual propagation speed. As described by Osher et al. (1982), there are six locations along the path in which such a change of sign is possible.

Since the linear transformation to characteristic variables is only applicable differences, the left cell values (L) are chosen as a reference state at each cell surface:

$$\tilde{Q}^*=\tilde{Q}_L+\sum_{\tilde{\alpha}}\Delta\tilde{Q}_{\tilde{\alpha}}g^{\tilde{\alpha}}; \tag{8}$$

where

$$\Delta\tilde{Q}_{\tilde{\alpha}}=\begin{cases}(\tilde{Q}^--\tilde{Q}_L)\cdot g_{\tilde{\alpha}} & \text{for } \lambda_c(\tilde{\alpha})>0\\ (\tilde{Q}^--\tilde{Q}_L)\cdot g_{\tilde{\alpha}} & \text{for } \lambda_c(\tilde{\alpha})\le 0\end{cases}$$

To prevent expansion shocks, the difference $\Delta\lambda_c(\tilde{\alpha})$ in the propagation speed between the two states $\tilde{Q}^+$ and $\tilde{Q}^-$ is calculated assuming a linear variation between both states:

$$\Delta\lambda_c(\tilde{\alpha})=\frac{\partial\lambda_c(\tilde{\alpha})}{\partial\tilde{Q}_{\tilde{\alpha}}}(\tilde{Q}^+-\tilde{Q}^-)_{\tilde{\alpha}} \tag{9}$$

The derivative is evaluated using the density weighted average. An expansion wave is indicated by a positive sign of the difference $\Delta\lambda_c(\tilde{\alpha})$ corresponding to one of the two characteristic pressure waves. The complete algorithm then becomes:

$$\Delta\tilde{Q}_{\tilde{\alpha}}=\begin{cases}(\tilde{Q}^--\tilde{Q}_L)\cdot g_{\tilde{\alpha}}+K & \text{for } \lambda_c(\tilde{\alpha})>0\\ \text{Eq. (8)} & \text{otherwise}\end{cases}, \tag{10}$$

where

$$K=min\left[1,\ max\left[0,\ \frac{1}{2}-\frac{\lambda_c(\tilde{\alpha})}{\Delta\lambda_c(\tilde{\alpha})}\right]\right]\times(\tilde{Q}^+-\tilde{Q}^L)\cdot g_{\tilde{\alpha}}$$

This is a highly accurate state difference splitting scheme, preventing unphysical solutions as known from the Roe's scheme (Harten et al., 1983), but using its simple algebra for the difference split. The components of the diffusive flux vector $\tilde{\underline{F}}^D\cdot g^i$ are approximated by central differences.

3.2 Time discretization

After evaluating the numerical flux vectors for a sequence of cells in the grid used in the manner outlined above, and to find the time accurate numerical solution to $\tilde{Q}(t)$ in Eq. (1), Eq. (6) has to be discretized in time through the use of a temporal difference scheme that approximates $\tilde{Q}$

(t) at discrete times. A general linear multi-step method to solve Eq. (6) takes the form

$$\sum_{j=0}^{m}\alpha_j\underline{\tilde{Q}}^{n+j}+\frac{\Delta t}{\Delta V}\sum_{j=0}^{m}\beta_j\sum_i\underline{\tilde{f}}^i(\underline{\tilde{Q}}^{n+j})S^i=0, \qquad (11)$$

where an approximation $\underline{\tilde{Q}}^{n+m}$ to $\underline{\tilde{Q}}(t^{n+m})$, a notation for the exact solution of Eq. (6) at the current discrete time t^{n+m}, is being sought. Δt denotes a constant time step size, i. e. $\Delta t=t^{n+m}-t^{n+m-1}$, and n denotes the discrete time index ($n=0, 1, 2, \cdots$). This method is called a m-step method ($m=1, 2, \cdots$), if $|\alpha_0|+|\beta_0|>0$. The coefficients α_j and β_j are fixed for a given method. A scheme given by Eq. (11) is called explicit if $\beta_m=0$, and implicit otherwise.

For implicit schemes ($\beta_m\neq 0$), a nonlinear system of equations of the form

$$\frac{\Delta V}{\Delta t}\alpha_m\underline{\tilde{Q}}^{n+m}-N(\underline{\tilde{Q}}^{n+m})=0 \qquad (12)$$

with

$$N(\underline{\tilde{Q}}^{n+m})=-\frac{\Delta V}{\Delta t}\sum_{j=0}^{m-1}\alpha_j\underline{\tilde{Q}}^{n+j}-\sum_{j=0}^{m}\beta_j\sum_i\underline{\tilde{f}}^i(\underline{\tilde{Q}}^{n+j})S^i$$

has to be solved for $\underline{\tilde{Q}}^{n+m}$ at each time step. The local accuracy of $\underline{\tilde{Q}}^{n+m}$ is determined by the order of the temporal difference scheme used. The three-point backward scheme ($m=2$, $\alpha_2=1.5$, $\alpha_1=-2.0$, $\alpha_0=0.5$, $\beta_2=1.0$, $\beta_0=\beta_1=0$) used here gives the local accuracy of second order. By contrast, the local accuracy of the backward Euler scheme ($m=1$, $\alpha_1=-\alpha_0=1$, $\beta_1=1$, $\beta_0=0$), frequently used for steady flow problems, is of first order.

At the beginning of computation ($t=n\Delta t=0$), a complete description of initial flow field $\underline{\tilde{Q}}(t^0)$ is needed at all the cells of the grid used. For a m-step method($m\geq 2$), the flow fields at previous time levels $m-1\leq n\leq 0$are additionally required, for which a $(m-1)$ step method is employed.

4. Solution Procedure

The choice made for attacking Eq. (12) at each time step has a profound effect on the efficiency of unsteady flow simulations. A well known method for attacking this problem is the Newton-Raphson method in which the Jacobian system is solved through the use of a direct or indirect method. However, the exact evaluation of the Jacobian is seldom the case in practice, and furthermore involves large storage. The solution procedure taken in the current work is based on the concept of defect correction scheme for nonlinear systems after Auzinger (1987). Applying the scheme to Eq. (12) and dropping the discrete time index $n+m$ for simplicity results in

$$\frac{\Delta V}{\Delta t}\alpha_m\underline{\tilde{Q}}^{\nu+1}-N(\underline{\tilde{Q}}^{\nu+1})=N(\underline{\tilde{Q}}^{\nu})-\tilde{N}(\underline{\tilde{Q}}^{\nu}) \qquad (13)$$

where $\tilde{N}(\underline{\tilde{Q}})$ is an approximation to $N(\underline{\tilde{Q}})$, and ν the nonlinear iterative index ($\nu=0, 1, 2, \cdots$). When this process converges, it provides $\underline{\tilde{Q}}^{n+m}$. The convergence property depends on the quality of $\tilde{N}(\underline{\tilde{Q}})$.

Linearizing Eq. (13) by the Taylor series expansion of order directly about $\underline{\tilde{Q}}^{\nu}$ yields

$$\left[\alpha_m\frac{\Delta V}{\Delta t}+\beta_m\frac{\partial\left[\sum_i\underline{\tilde{f}}^i(\underline{\tilde{Q}}^{\nu})S^i\right]}{\partial\underline{\tilde{Q}}^{\nu}}\right]\Delta\underline{\tilde{Q}}^{\nu}$$
$$=N(\underline{\tilde{Q}}^{\nu})-\alpha_m\frac{\Delta V}{\Delta t}(\underline{\tilde{Q}}^{\nu})+O[(\Delta\underline{\tilde{Q}}^{\nu})^2] \qquad (14)$$

Since $\underline{\tilde{Q}}^{n+m}$ is determined only by the right hand side of Eq. (14), and the linearization error vanishes if this iterative process converges, i. e. $\Delta\underline{\tilde{Q}}^{\nu}\approx 0$, this iterative process is fully conservative in time. Such a conservative property is necessary for unsteady flows in which time accurate solutions are of interest. For the flux Jacobians on the left hand side of Eq. (14), the first order flux difference splitting after Roe (1981) is employed. The first order differencing of the convective flux function enters more diffusion acting on the residual than higher order differencing, thus enhancing stability.

The control volume under consideration consists of different types of boundaries, and appropriate conditions are thus needed to solve Eq. (12). All the boundary conditions used here take the form

$$a(\underline{\tilde{Q}})=a_{target} \qquad (15)$$

with a being a physical quantity or its extrapolation function. To make Eq. (15) consistent with Eq. (14), the linearization of Eq. (15) is made

$$\frac{\partial a(\tilde{Q}^{\nu})}{\partial \underline{Q}^{\nu}} \Delta \underline{\tilde{Q}}^{\nu} = a_{target} - a(\underline{\tilde{Q}}^{\nu}) \tag{16}$$

Combining Eqs. (14) and (16) yields a vector equation of the form

$$[A]^{\nu} \Delta \underline{\tilde{Q}}^{\nu} = RHS(\underline{\tilde{Q}}^{\nu}) \tag{17}$$

with

$$\underline{\tilde{Q}}^{\nu+1} = \underline{\tilde{Q}}^{\nu} + \varsigma \Delta \underline{\tilde{Q}}^{\nu},$$

where $\varsigma \in (0, 1]$ is the step size length that may be a fixed value or chosen adaptively to minimize $\Delta \underline{\tilde{Q}}^{\nu}$ rapidly, thus ensuring convergence. The vector $RHS(\underline{\tilde{Q}}^{\nu})$ represents the residual that vanishes at each time step if this iterative process converges. Eq. (17) stands for a sequence of linear systems of equations, with coefficient-matrix $[A]$ being block-structured and asymmetric, to be solved at each time step, and the solution of which often makes up most of the work involved in the determination of $\underline{\tilde{Q}}^{\nu} (\approx \underline{\tilde{Q}}^{n+m})$ satisfying $RHS(\underline{\tilde{Q}}^{\nu}) \approx 0$.

The computing costs of the iterative process of Eq. (17) depend greatly on the quality of the initial guess $\underline{\tilde{Q}}^{\nu=0}$. To provide a good initial guess at each time step, an implicit formula of the form

$$\underline{\tilde{Q}}^{\nu=0} = \sum_{j=0}^{m} \beta_j \underline{\tilde{Q}}^{n+j-1} + \sum_{j=0}^{m} \alpha_j \underline{\tilde{Q}}^{n+j-1} \tag{18}$$

is used as a predictor. The convergence criterion of the iterative process of Eq. (17) adopted in this work relies on the root mean square (RMS) of the residual $RHS(\underline{\tilde{Q}}^{\nu})$. The next time stepping is then tackled when a value of RMS meets a specified error of tolerance.

A technique for improving the overall efficiency of the Newton-Raphson method is to construct and to factorize the Jacobian matrix once at the beginning of the Newton-Raphson iteration, and thus the matrix factorized once is used repeatedly. Although this technique may decrease the rate of convergence, it increases a certain measure of efficiency when the Jacobian matrix is not changing rapidly. Such an idea would be applicable to the process of Eq. (17), resulting in

$$[A]^{\nu=0} \Delta \underline{\tilde{Q}}^{\nu} = RHS(\underline{\tilde{Q}}^{\nu}) \tag{19}$$

with

$$\underline{\tilde{Q}}^{\nu+1} = \underline{\tilde{Q}}^{\nu} + \varsigma \Delta \underline{\tilde{Q}}^{\nu} \text{ and}$$
$$[A] = [L] + [D] + [U],$$

where $[D]$ is the block-diagonal of $[A]$, $[L]$ and $[U]$ are strictly lower and upper triangular matrices, respectively.

4.1 Defect correction scheme

The exact solution of the Jacobian system of Eq. (17) at each ν in terms of a direct method gives rise to very costly arithmetic operations and high storage requirements, and would not necessarily yield a high efficiency. Therefore, it seems reasonable to solve the system iteratively because the coefficient-matrix $[A]$ is good-conditioned for iterative methods requiring lower core memory. The majority of iterative approaches taken in practice for linear systems are based on the defect and the correction.

Suppose there exist a nonsingular matrix $[K]^{\nu}$ that is an approximation to $[A]^{\nu}$, but unlike $[A]^{\nu}$, readily invertible, the linear system Eq. (17) is then clearly equivalent to

$$[K]^{\nu} \Delta \underline{\tilde{Q}}^{\nu} = ([K]^{\nu} - [A]^{\nu}) \Delta \underline{\tilde{Q}}^{\nu} + RHS(\underline{\tilde{Q}}^{\nu}) \tag{20}$$

that leads to the iterative defect correction scheme

$$\begin{aligned} [K]^{\nu} \delta \underline{\tilde{Q}}^{\kappa} &= RHS(\underline{\tilde{Q}}^{\nu}) - [A]^{\nu} \Delta \underline{\tilde{Q}}^{\nu,\kappa} \\ &= res(\Delta \underline{\tilde{Q}}^{\nu,\kappa}) \end{aligned} \tag{21}$$

with

$$\Delta \underline{\tilde{Q}}^{\nu,\kappa+1} = \delta \underline{\tilde{Q}}^{\kappa} + \Delta \underline{\tilde{Q}}^{\nu,\kappa},$$

where χ is the linear iteration index ($\chi = 1, 2, \cdots$), $res(\Delta \underline{\tilde{Q}}^{\nu,\kappa})$ the defect and $\delta \underline{\tilde{Q}}^{\kappa}$ the correction.

Since we are interested only in the overall efficiency for finding a vector $\underline{\tilde{Q}}^{\nu} (\approx \underline{\tilde{Q}}^{n+m})$ satisfying $RHS(\underline{\tilde{Q}}^{\nu}) \approx 0$ at every time step, it is not necessary to solve Eq. (17) at every iteration ν. We only seek to obtain an approximation of $\Delta \underline{\tilde{Q}}^{\nu}$ yielding the best nonlinear convergence, so a question arises how to terminate the iterative process of Eq. (21) for a satisfactory nonlinear convergence rate. In this work, the iterative process is thus stopped at every iteration ν when $\Delta \underline{\tilde{Q}}^{\nu,\kappa}$ satisfies

$$\frac{\| res(\Delta \underline{\tilde{Q}}^{\nu,\kappa}) \|_2}{\| RHS(\underline{\tilde{Q}}^{\nu}) \|_2} \leq \phi \tag{22}$$

where $\phi \in [0, 1)$ is a forcing factor that is used to control the level of the solution accuracy to Eq. (17).

The forcing vector ϕ offers a trade-off between the accuracy with which the linear system of Eq. (17) is solved and the amount of the work at every nonlinear iteration ν. The question is what level of accuracy is required to preserve the optimal nonlinear convergence. The choice of ϕ depends on different factors, such as the time stepping scheme used, form of the implicit operator, time step size Δt, step size length ς and the characteristics of flows under consideration.

The choice of the matrix $[K]^{\nu}$, called the splitting matrix, determines a linear iterative procedure. The linear solver used in this work is the incomplete point factorization taking the form of the splitting matrix

$$[K]^{\nu}=([L]^{\nu}+[D_0]^{\nu})[D_0^{-1}]^{\nu}([D_0]^{\nu}+[U]^{\nu}) \tag{23}$$

where $[D_0]$ is also a block-diagonal matrix. The exact evaluation of $[D_0]$ to satisfy $([A]-[K])$ is equivalent to a complete factorization. The splitting matrix of the incomplete factorization method requires to satisfy the block-diagonal of $([A]-[K])$ is equal to

$$[D_0]^{\nu}=[D]^{\nu}-blockdiagonal([L]^{\nu}[D_0^{-1}]^{\nu}[U]^{\nu}) \tag{24}$$

Setting $[D_0]^{\nu}=[D]^{\nu}$, the splitting matrix of Eq. (24) becomes that of the symmetric point Gauss-Seidel method. The evaluation and factorization of $[D_0]^{\nu}$ are carried out once at the beginning of the process of Eq. (21) because $[A^{\nu}]$ remains unchanged during the process. When, moreover, using the frozen Jacobian matrix of Eq. (19), the block-diagonal $[D_0]^{\nu}$ is factorized once at the beginning of the iterative process of Eq. (19) since $[A]^{\nu=0}$ remains unchanged for each time step. This incomplete point factorization scheme is taken advantage of as a smoother in the correction storage scheme that will be described in the following.

4.2 Correction storage scheme

The multigrid technique proved to be one of the most effective methods for accelerating convergence of steady flow solvers. This iterative multigrid method was originally developed (Brandt, 1977) to solve the discrete form of elliptic differential equations, for which conventional iterative methods are known to converge rapidly for a first few iterations and very slowly thereafter. Fourier analysis of the error reduction process (Brandt, 1977) shows that usual iterative methods are efficient in smoothing out errors of wavelengths comparable to the grid spacing, but are insufficient in liquidating long wavelength components. Thus the process of annihilating long wave errors is characterized by a slow rate of convergence.

To realize the fact that a wavelength is longer relative to a fine mesh than relative to a coarse mesh, the multigrid method makes use of different grids to remove different wavelength errors. Consequently, the multigrid technique cycles between coarser and finer grids until all the wavelength errors are appropriately smoothed out. This process greatly speeds up the convergence of usual iterative methods. Moreover, solving on coarser grids requires far less computational effort, since the grid points are fewer.

This multigrid idea may be applied to the solution of a form of system of algebraic equations arising at each implicit time stepping. With multigrid methods, the computation is conducted on a sequence of grids G_l, where $l=1, 2, 3, \cdots, L$, with $l=L$ representing the finest grid on which the desired solution is being sought, and the grids become coarser as the level of l smaller. The coarser grids are formed by eliminating every other grid line in each direction on the previous finer grid.

Such a multigrid idea may be applied directly to the nonlinear system of Eq. (12) at each time step (full approximate storage scheme). Instead, the multigrid method taken in this work is the correction storage scheme applied indirectly to a sequence of linear systems with the frozen Jacobian matrix of Eq. (19) to solve the nonlinear system of Eq. (12) under the boundary conditions of Eq. (15).

Let

$$[A]_l^{\nu=0}\underline{x}_l = rhs(\underline{x}_l) \tag{25}$$

with

$$[A]_{l=L}^{\nu=0} = [A]^{\nu=0},\ \underline{x}_{l=L} = \Delta\underline{\tilde{Q}}^{\nu},$$
$$rhs(\underline{x}_{l=L}) = RHS(\underline{\tilde{Q}}^{\nu})$$

denotes a linear system on G_l and $\underline{\tilde{x}}_l^{old}$ an approximation of $\underline{x}_l$, obtained through a few iterations on G_l. Then the solution error $\underline{e}_l = \underline{x}_l - \underline{\tilde{x}}_l^{old}$, called the correction, satisfies the following relationship:

$$[A]_l^{\nu=0}\underline{e}_l = rhs(\underline{x}_l) - [A]_l^{\nu=0}\underline{\tilde{x}}_l^{old} = res(\underline{e}_l) \tag{26}$$

In the correction storage scheme, an estimate of $\underline{e}_l$ is obtained by solving the coarse grid system

$$[A]_{l-1}^{\nu=0}\underline{e}_{l-1} = I_l^{l-1} res(\underline{e}_l) = rhs(\underline{e}_{l-1}) \tag{27}$$

on grid G_{l-1} and interpolating its approximation to G_l, where I_l^{l-1} is a transfer operator for the residual $res(\underline{e}_l)$ from G_l to G_{l-1}.

Since solving the fine-grid system of Eq. (25) with an arbitrary initial guess is equivalent to solving the corresponding residual system of Eq. (26) with the initial guess $\underline{e}_l = 0$, it is thus desirable to initiate the iteration on the coarse-grid system of Eq. (27) with the initial guess $\underline{e}_{l-1} = 0$. An approximation $\underline{\tilde{e}}_{l-1}$ to the solution of Eq. (27), obtained through a few iterations on G_{l-1}, is transferred to grid G_l, and then it comes to

$$\underline{\tilde{x}}_l^{new} = \underline{\tilde{x}}_l^{old} + \omega_l I_{l-1}^l \underline{\tilde{e}}_{l-1} \tag{28}$$

where I_{l-1}^l denotes a transfer operator for $\underline{\tilde{e}}_l$ from G_{l-1} to G_l. On G_l, some iterations are initiated with the better approximation $\underline{\tilde{x}}_l^{new}$ on Eq. (25). The step length factor

$$\omega_l = \frac{(rhs(\underline{\tilde{e}}_{l-1}),\ \underline{\tilde{e}}_{l-1})}{([A]_{l-1}^{\nu=0}\underline{\tilde{e}}_{l-1},\ \underline{\tilde{e}}_{l-1})} \tag{29}$$

is chosen so that the estimate $\underline{\tilde{e}}_l$ is improved (Hackbusch et al., 1989).

This process is recursive. If convergence slows down for Eq. (27), or G_{l-1} is large, $res(\underline{e}_{l-1})$ is then transferred to G_{l-2}, etc.. On G_1, one solves the coarse grid system either directly or iteratively until its solution is sufficiently approximated. This schedule for the grids in the order in which they are visited is called the V-cycle.

The choice of an iterative smoothing scheme plays a crucial role of the effectiveness of the multigrid technique, but somewhat problem dependent. In this work, the incomplete point factorization method described above is made use of as a smoothing scheme. The coefficient-matrix $[A]_l$ on the coarse grid $G_l (l<L)$ is generated approximately through the injection of $\underline{\tilde{Q}}_{l+1}^{\nu=0}$ to the implicit operator of Eq. (14). The construction of the coefficient-matrix $[A]_l^{\nu}$ and the block-diagonal matrix $[D_0]_l$, and the factorization of $[D_0]_l$ are performed only once on each grid G_l for a time step, thus the factorized matrix is reused repeatedly. Only one V-cycle with $L=2$ and a smoothing iteration before restriction and after interpolation, respectively, is carried out because the iterative process of Eq. (19) does not require a high accurate linear solution at each nonlinear iteration ν.

With regard to the transfer operator I_l^{l-1} the full weighting is used, but the injection at boundaries:

$$I_l^{l-1} res(\underline{e}_l) = \frac{1}{16}\begin{bmatrix} 1 & 2 & 1 \\ 2 & 4 & 2 \\ 1 & 2 & 1 \end{bmatrix} res(\underline{e}_l) \tag{30}$$

and

$$I_l^{l-1} res(\underline{e}_l) = res(\underline{e}_l) \tag{31}$$

and the transfer of $\underline{\tilde{e}}_{l-1}$ from G_{l-1} to G_l is performed with the aid of a linear interpolation:

$$I_{l-1}^l \underline{\tilde{e}}_{l-1} = \frac{1}{4}\begin{bmatrix} 1 & 2 & 1 \\ 2 & 4 & 2 \\ 1 & 2 & 1 \end{bmatrix} \underline{\tilde{e}}_{l-1} \tag{32}$$

The correction storage scheme described until now is limited to linear problems because the relationship of Eq. (26) is valid only for such problems. By contrast, since the full approximate storage scheme approximates the solution $\underline{x}_{l-1} = \underline{\tilde{x}}_{l-1} + \underline{e}_{l-1}$ on G_{l-1}, this scheme is applicable independent of linearity, but slightly more expensive when applying to linear problems.

5. Results and Discussion

The test case chosen is the two-dimensional unsteady laminar flow of an ideal gas past a circular cylinder of diameter L_∞ that moves with a constant velocity of U_∞ following an impulsive start in the direction $\theta = \pi$ at time $t=0$ from rest.

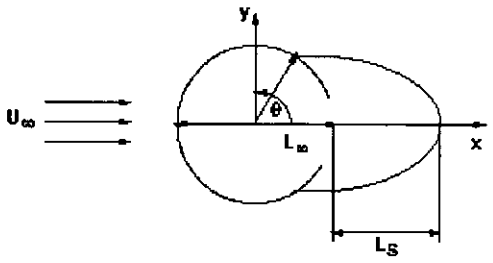

Fig. 1 Dimensional geometry of the problem

The impulsive motion is modeled with an abrupt change of Reynolds number of a flow past the cylinder at rest. Therefore, the translational velocity U_∞ of the cylinder corresponds to a uniform flow at infinity in the direction $\theta=0$, sketched in Fig. 1.

The characteristics of such flow are well known from measurements (Bouard et al., 1980; Roshko, 1953). For a range of reference Reynolds numbers $6 \leq Re_\infty \leq 40 (Re_\infty = \rho_\infty U_\infty L_\infty / \mu_\infty)$, the flow reaches a steady state, with a pair of symmetric vortices at the rear of the cylinder. On the other hand, at higher Reynolds numbers stable symmetric flow exists only for a relatively short period of time, followed by a periodic vortex shedding flow, transforming into the so-called von Karman vortex street.

At very low local Mach numbers ($Ma \ll 1$), the change in density is negligible. The flow under consideration here is thus assumed to meet the incompressible conditions reasonably, under which computed results can be compared with the measurements present. Throughout the work, computations were done for a reference Mach number of $Ma_\infty=0.1$ on a 85×235 O-grid with clustering of the grid points near the surface of the cylinder and in the wake region.

The minimum grid spacing at the wall is 0.1% of L_∞. The time integration was made by means of the three-point backward scheme of second order accuracy. The time step size Δt and the step length factor ς are limited due to the nonlinear convergence problem, and thus the maximum values to be allowed, $\Delta t=0.01$ and $\varsigma=0.65$, are taken for all the computations. Along with the time step size Δt, the size of ς depends on the Reynolds number Re_∞, the Mach number Ma_∞ and the grid used, etc. .

For initial conditions at $t=0$, the analytic solution for incompressible potential flow was imposed on the entire flow field. There are three different types of boundary conditions; inflow, outflow and solid surface. On the solid surface, the no-slip, the static pressure and temperature of zero order were applied. At the outflow, the mass density was kept constant, the momentum densities and the total temperature were extrapolated from the interior. At the inflow, the total temperature and the total pressure, and a momentum density were imposed, the other momentum density was extrapolated. At each time step, computations were carried out until a value of RMS for $RHS(\underline{\tilde{Q}}^\nu)$ in Eq. (19) fell below a designated value of 10^{-6}, which required $\nu \approx 3\sim4$ per time step. The solution thus at each time step obtained was considered as accurate enough, and then the next time stepping was tackled.

The important functionals for the flow past a cylinder are the time evolutions of forces exerted by the fluid on the cylinder. The drag coefficient C_D and the lift coefficient C_L at some instant in time t are obtained by integrating the wall pressure p_w and the wall vorticity $\xi_w (\xi = \partial u/\partial y - \partial v/\partial x)$ around the cylinder surface:

$$C_D = -\int_0^{2\pi} p_w \cos\theta d\theta + \frac{\mu}{Re_\infty}\int_0^{2\pi} \xi_w \sin\theta d\theta, \tag{33}$$

$$C_L = -\int_0^{2\pi} p_w \sin\theta d\theta - \frac{\mu}{Re_\infty}\int_0^{2\pi} \xi_w \cos\theta d\theta, \tag{34}$$

where the first and the second terms of the two Eqs. (33) and (34) correspond to the contributions of the static pressure and the skin friction forces, respectively.

Immediately after impulsive start, vortices are created on the surface of the cylinder to meet the no-slip conditions. The integrals of Eqs. (33) and (34) are numerically evaluated through the use of the trapezoidal rule. The periodicity of vortex shedding is expressed by the Strouhal number ($Str = 1/T$), where T is the period of vortex shedding.

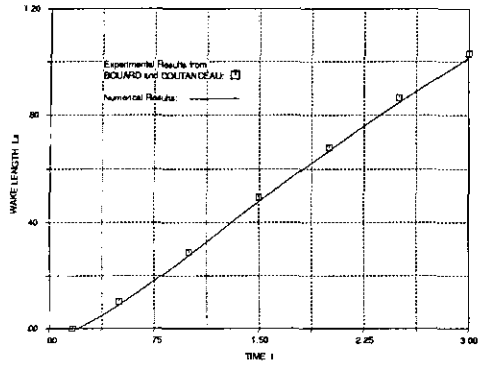

(a) $Re_\infty=550$

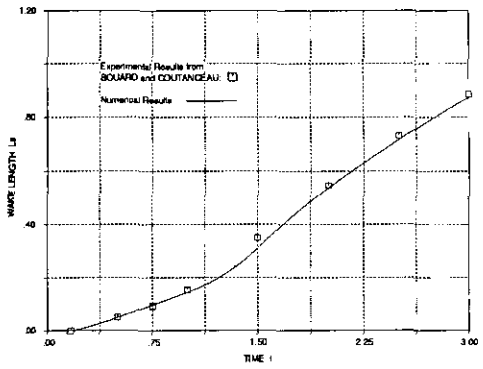

(b) $Re_\infty=3000$

Fig. 2 Time evolution of the main closed wake length

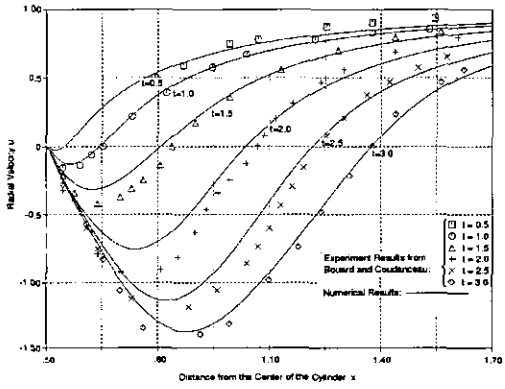

Fig. 3 Time evolution of the radial velocity on the symmetry axis for $Re_\infty=3000$

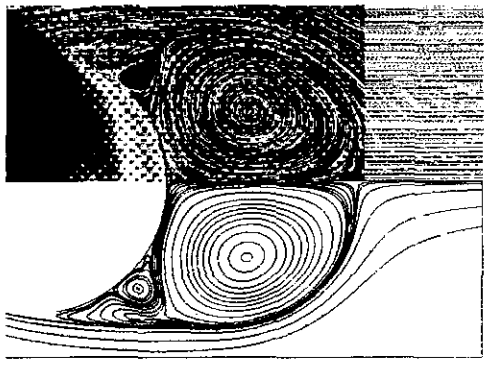

Fig. 4 Flow structure for $Re_\infty=3000$ at $t=2.5$

5.1 Flow development

5.1.1 Flow at initial phase

The flow development with time at the initial stage $0\leq t\leq 3$ is first presented along with the comparison with measurements of Bouard et al. (1980). The time evolutions of the main closed wake lengths at $Re_\infty=550$ and 3000 are given in Figs. 2(a) and 2(b). The numerical predictions agree relatively well with the measured data.

As shown in Fig. 3, for $Re_\infty=3000$, the time evolutions of the radial velocity distributions on the symmetry axis behind the cylinder are plotted and compared with the measured data and show a reasonable agreement. The negative values of velocity mean the reversal flow in the primary wake, the existence of values of velocity modulus greater than can be shown. The computed results somewhat differ from the measured data. This discrepancy could be attributed to the initial conditions (Loc et al., 1985), for which an incompressible potential flow field was imposed here. Figure 4 shows a good agreement of the flow field in the half wake, depicted with the computed streamlines and the experimental pathlines for at $Re_\infty=3000$ at $t=2.5$.

5.1.2 Vortex shedding

For a Reynolds number above $Re_\infty=40$, after a certain lapse of time following the initial symmetric phase, an arrangement of vortices are alternatively shed from the rear of the cylinder. The vortices thus separated are convected and diffused in the wake, evolving toward a periodic configuration, the so-called von Karman vortex street.

A way to generate a vortex shedding flow within a reasonable time is to impose some artificial perturbation on the flow field (Lecointe et al., 1984; Patel, 1978); the destabilization of the flow is triggered by rotating the cylinder for a period

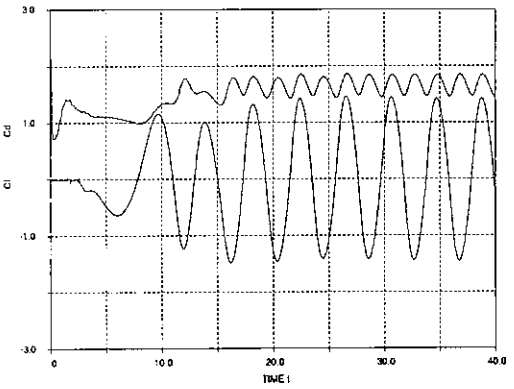

Fig. 5 Time evolution of the lift and the drag coefficients for $Re_\infty = 1000$

of time in the clockwise and then in the counterclockwise directions.

In the present work also, only a fully developed alternating vortex shedding flow with some periodicity are of interest, an artificial perturbation is thus introduced in the flow field in the following way:

$$u_w = \begin{cases} 0.15 \text{ for } 1.5 \le t \le 1.75 \\ -0.25 \text{ for } 1.75 < t < 2.5 \end{cases} \tag{35}$$

where u_w is the circumferential velocity of the surface of the cylinder. The present computation was made for $Re_\infty = 10^3$ up to $t = 30$ at which time a periodic vortex shedding flow is fully developed.

Figure 5 describes the time evolutions of the lift and the drag coefficients. The periodic properties of the flow can clearly be observed by the time evolution of the lift coefficient. The period of the oscillations is found to be 4.473, resulting in the Strouhal number Str equal about 0.22. This result agrees very well with the scattered experimental values in the range of 0.21~0.22 reported by Roshko (1953) although the present computation predicts a slightly higher Strouhal number. The time evolution of the drag, coefficient, essentially a flow loss, is not alternating but periodic. The frequency of the oscillations of the drag coefficient is found to be twice that of those of the lift coefficient. This is due to the contributions of the upper and the lower alternating vortices to the drag force.

Let t^* some instant in time at which the lift

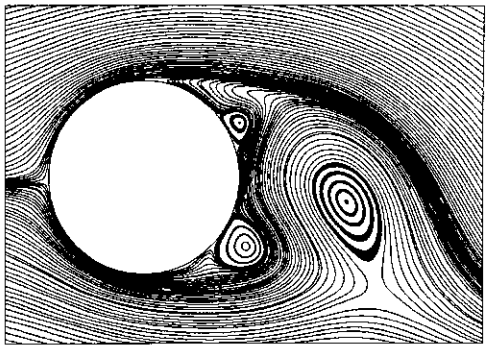

Fig. 6 Instantaneous streamlines at $t = t^* + T/4$ for $Re_\infty = 1000$

coefficient is maximal. The maximal positive lift coefficient is produced due to a large vortex of a low pressure field attached to the upper side of the cylinder at $t = t^*$, the maximal drag coefficient as well. With lapse of time the vortex is shed from the cylinder, forming the upper vortex of the von Karman vortex street. The lift coefficient is zero and the drag coefficient is minimal at $t = t^* + T/4$. At $t = t^* + T/2$ another large vortex, opposite to that at the upper side in rotation, is again created at the lower side of the cylinder, reversing the direction of the lift coefficient. This vortex is also swept into the wake region, forming the lower vortex of the von Karman vortex street. In Fig. 6, a flow state at $t = t^* + T/4$ is depicted by the instantaneous streamlines, and is a mirror image of that at $t = t^* + 3T/4$.

5.2 Comparison of solution procedures

To make a comparison of the effectiveness for different solution procedures, the alternating vortex shedding flow at $Re_\infty = 10^3$ was considered as a test example. The comparison was made up to $t = 30$ at which time the periodic alternating vortex shedding flow was fully developed. The local computational cost differs at every time step since the flow structure changes with lapse of time. Thus, the total computational labor for a period of time does not correspond to the local effort along the time step times the number of time steps. For consistent comparison, the incomplete point factorization method was taken as a linear solver with a stopping criterion on the single grid and as a smoother on the multigrid. To our

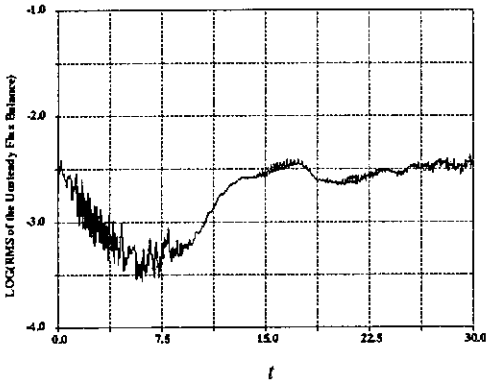

Fig. 7 Time evolution of RMS for the unsteady numerical flux balance

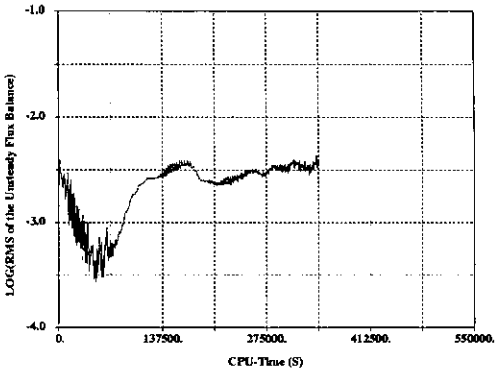

Fig. 9 Single grid method with freezing Jacobian matrix.

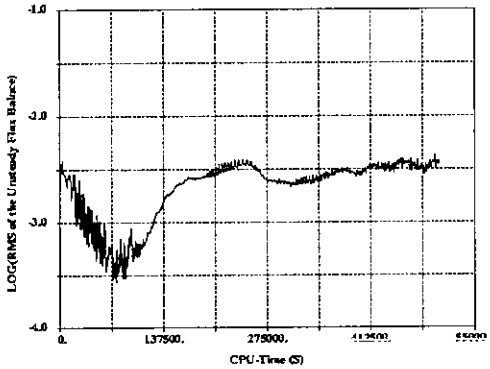

Fig. 8 Single grid method without freezing Jacobian matrix.

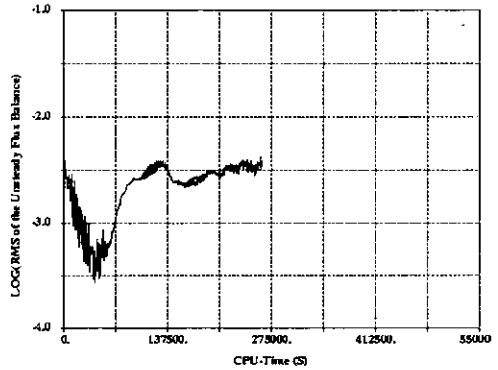

Fig. 10 Correction storage method with freezing Jacobian matrix.

experience, $\phi=0.1$ was the best choice for the single grid in the test case. In each computation, the root mean square (RMS) for the unsteady numerical flux balance is plotted versus computing cost, given in central processing unit (CPU) seconds (S) on one processor of a HP9000/K400 parallel computer.

Figure 7 shows the time evolution of RMS for the unsteady numerical flux balance, the second term of Eq. (6), which vanishes at steady state. It follows that after a lapse of time following the initial phase, the flow is strongly unsteady. Figures 8-10 indicate the behavior of RMS for the numerical flux balance versus computing time for different solution procedures. On the single grid first, by comparison of computing costs in Figs. 8 and 9, it can be shown that computing costs may be saved in terms of the frozen Jacobian matrix, to a great extent. Only once at the beginning of the iterative process of Eq. (19) at each time step, the Jacobain matrix is evaluated and the diagonal associated with the incomplete point factorization method is factorized. Then the resulting matrix is reused during the solution process of a sequence of linear systems. No difficulties encountered with the frozen Jacobian matrix were experienced in the nonlinear convergence when using the values of Δt, S and $\underline{Q}^{\nu=0}$ aforementioned above.

For the case of multigrid method, in addition, the effect of freezing the Jacobian matrix on the overall efficiency was checked up. The nonlinear process of Eq. (19) used in the current work does not checked up the efficiency. The nonlinear iterative require highly accurate linear solutions. Thus, only a coarse grid was made use of approximately to obtain solution errors generated by initiating an iteration on the fine grid. One of the major efforts in the correction storage scheme is

to construct the coefficient-matrix and factorize the diagonal associated with the smoothing iterative method on the coarse grid. When the frozen Jacobian matrix on the coarse grid is used, a marked improvement in computational efficiency could be obtained. By comparison of the solution procedures with the frozen Jacobian matrix on the single grid and the multigrid, from Figs. 9 and 10, it follows that by 20% of computing time required to obtain a fully developed vortex shedding flow can be saved by means of the correction storage scheme. To conclude, the correction storage scheme with the frozen Jacobian matrix is much more efficient when compared with the solution procedures without freezing the Jacobian matrix on the single grid.

6. Conclusions

A correction storage scheme for solving a sequence of approximate Jacobian systems arising at each implicit time step were implemented and tested for a unsteady flow past a circular cylinder.

The code for the simulation of unsteady flow was validated against the measured data present. In the test case, the computed results showed a reasonable agreement with the experiments at the fully developed periodic stage as well as the initial symmetric stage.

With regard to the effectiveness of the solution procedures tested here, computing costs may be saved in favor of freezing the Jacobian matrix on the single grid, to a great extent. Furthermore, through the combination of the correction storage scheme with the frozen Jacobian matrix a certain measure of computational efficiency could be acquired by comparison with the single grid method.

References

Auzinger, W., 1987, "Defect Correction for Nonlinear Elliptic Difference Equations," *Numerische Mathematik*, Vol. 51, pp. 199~208.

Bourad, R. and Coutanceau, M., 1980, "The Early Stage of Development of the Wake behind an Impulsively Started Cylinder for $40<Re<10^4$," *Journal of Fluid Mechanics*, Vol. 101, Part 3, pp. 583~607.

Brandt, A., 1977, "Multi~Level Adaptive Solutions to Boundary Value Problems," *Mathematics of Computation*, Vol. 31, No. 138, pp. 333~390.

Breuer, M. and Haenel D., 1993, "A Dual Time Stepping Method for 3~D, Viscous Incompressible Vortex Flows," *Computers and Fluids*, Vol. 22, No. 4/5, pp. 467~484.

Dailey, L. D. and Pletcher, R. H., 1996, "Evaluation of Multigrid Acceleration for Precon -ditioned Time-Accurate Navier-Stokes Algorithms," *Computers and Fluids*, Vol. 25, No. 8, pp. 791~811.

Deniss, S. R. and Chang, G. -Z., 1970, "Numerical Solutions for Steady Flows past a Circular Cylinder at Reynolds Numbers up to 100," *Journal of Fluid Mechanics*, Vol. 42, Part 3, pp. 471 ~489.

Hackbusch, W., and Reusken, A., 1989, "Analysis of a Damped Nonlinear Multilevel Method," *Numerische Mathematik*, Vol. 55, pp. 225~246.

Harten, A. and Hyman, J. M., 1983, "Self Adjusting Grid Methods for One-Dimensional Hyperbolic Conservation Laws," *Journal of Computational Physics*, Vol. 50, pp. 235~269.

Jameson, A., 1991, "Time Dependent Calculations Using Multigrid, with Applications to Unsteady Flows past Airfoils and Wings," *AIAA Paper 91~1596*.

Jiang H. and Forsyth P. A., 1995, "Robust Linear and Nonlinear Strategies for Solution of the Transonic Euler Equations," *Computers and Fluids*, Vol. 24, No. 7, pp. 753~770.

Lecointe, Y. and Piouet, J., 1984, "On the Use of Several Compact Methods for the Study of Unsteady Incompressible Viscous Flow round a Circular Cylinder," *Computers and Fluids*, Vol. 12, No. 4, pp. 255~280.

Loc, T., P., 1980, "Numerical Analysis of Unsteady Secondary Vortices Generated by an Impulsively Started Circular Cylinder," *Journal of Fluid Mechanics*, Vol. 100, Part 1, pp. 111 ~128.

Loc, T., P. and Bouard, R., 1985, "Numerical Solution of the Early Stage of the Unsteady

Viscous Flow around a Circular Cylinder: a Comparison with Experimental Visualization and Measurements," *Journal of Fluid Mechanics*, Vol. 160, pp. 93~117.

Osher, S. and Solomon, F., 1982, "Upwind Schemes for Hyperbolic Systems of Conservation Laws," *Mathematics of Computation*, Vol. 38, pp. 339~377.

Patel, V. A., 1978, "Karman Vortex Street behind a Circular Cylinder by a Series Truncation Method," *Journal of Computational Physics*, Vol. 28, pp. 14~42.

Pulliam, T., 1993, "Time accuracy and the Use of Implicit Methods," *AIAA Paper 93~3360 ~CP*.

Rai, M., 1989, "Three~Dimensional Navier-Stokes Simulations of Turbine Rotor-Stator Interaction, Part I -Methodology," *Journal of Propulsion and Power* 5,307.

Reichert, A. W. and Simon, H., 1994, "Numerical Investigation on the Optimum Design of Radial Inflow Turbine Guide Vane," *ASME Paper 94~GT~61*.

Roe, P. L., 1981, "Approximate Riemann Solvers, Parameter Vectors and Difference Schemes," *Journal of Computational Physics*, Vol. 43, pp. 357~372.

Roshko, A., 1953, "On the Development of Turbulent Wakes from Vortex Streets," *NACA TN 2913*.

Sheng, C., T. and Whitfield, A., 1995, "A Multigrid Algorithm for Unsteady Incompressible Euler and Navier~Stokes Flow Computations," *Sixth Int. Symp. on Computational Fluid Dynamics*, Vol. Ⅲ, pp. 1123~1128.

Van Albada, G. D., van Leer, B. and Roberts B. B., 1982, "A Comparative Study of Computational Methods in Cosmic Gasdynamics," *Astronomy and Astrophysics*, Vol. 108, pp. 76~84.